

# Wave-function entropy and dynamical-symmetry breaking in the interacting boson model

Pavel Cejnar<sup>1</sup> and Jan Jolie<sup>2</sup>

<sup>1</sup>*Dept. of Nuclear Physics, Charles University, V Holešovičkách 2,*

*CZ—180 00 Prague, Czech Republic*

<sup>2</sup>*Dept. of Physics, University, P erolles, CH—1700 Fribourg, Switzerland*

(September 18, 2018)

## Abstract

The degree of chaos in the Interacting Boson Model (IBM-1) is compared with what we call the “dynamical-symmetry content” of the system. The latter is represented by the information entropy of the eigenfunctions with respect to bases associated with dynamical symmetries of the IBM-1, and expresses thus the localization of actual eigenfunctions in these symmetry bases. The wave-function entropy is shown to be a sensitive tool for monitoring the processes of a single dynamical-symmetry breaking or transitions between two and more symmetries. For the IBM-1 hamiltonians studied here, the known features related to chaos, namely the dependence of chaotic measures on the hamiltonian parameters (position in the Casten triangle) and on the angular momentum, turn out to be correlated with the behaviour of the wave-function entropy.

21.60.Fw; 05.45.+b

## I. INTRODUCTION

Although fundamental quantum-mechanical equations of motion are about seventy years old, the task to understand the whole variety of phenomena “encoded” in them has not been completed yet. One of the most interesting problems of this sort is to find quantum signatures of the order-to-chaos transition: If the dynamics of a classical system is changed, by varying some parameters, from the regular to chaotic regime, what happens on the level of the system’s quantum counterpart? Much insight into the classical–quantum correspondence has been gained in connection with this question in recent years [1], but many problems still remain open.

It is well known that the order/chaos signatures can be found in both the factors that determine quantum dynamics of any bound system, i.e., in both discrete sets of (i) energy eigenvalues and (ii) corresponding eigenfunctions. The transition to chaos in the classical limit was found to set up specific short- and long-range correlations in the energy spectrum and a regime of Gaussian overlaps of the energy eigenfunctions with any probe state [2]. Besides these properties, inherently described by random–matrix theory [3], also certain spatial and temporal properties of wave functions (such as nodal-line patterns, scars, wave-packet dynamics etc.) were shown to be affected by the order-to-chaos transition [1].

Regularity and chaos are sometimes thought as limiting manifestations of various degrees of symmetry contained in the system [4]. Indeed, regularity is obviously related to integrability (integrable systems are always totally regular) and the latter, since it ensures a number of compatible integrals of motion, is nothing else than “a kind of symmetry”. When dealing with symmetries, we do not have in mind exact symmetries that the system can exhibit, but rather the generalized, so-called dynamical symmetries [5–9]. Although dynamical symmetries are defined only for algebraic systems (i.e., systems associated with a dynamical group  $G$  whose representations define the system’s Hilbert space and whose generator algebra induces all the relevant operators on this space), their role in physics is probably quite general.

A system with a dynamical group  $G$  has a dynamical symmetry if its hamiltonian can be written exclusively in terms of Casimir operators of the subgroups involved in the chain

$$G \supset G_1 \supset \dots \supset G_i \supset \dots \supset G_k , \quad (1)$$

which specifies the given dynamical symmetry. Note that only the smallest embedded group,  $G_k$ , is an ordinary symmetry group. The systems with dynamical symmetries have two rather exclusive properties: First, their eigenspectra and corresponding eigenfunctions can be found analytically [6] and, second, they are integrable [8–11]. However, also known is that, in turn, integrability *does not* have to always couple with dynamical symmetries, which means that the link of the present concept of symmetry to chaos is still imperfect.

In spite of the above-mentioned numerous signatures of quantum chaos found in recent years, very little has been said about the connection of the quantum order-to-chaos transition with the process of dynamical-symmetry breaking. In particular, the question should be addressed “to what extent” a concrete dynamical symmetry must be broken to induce the transition to chaos [11]. An obvious problem is that whereas dynamical symmetry (and integrability) follows a simple boolean logic—the system either has it or not—the order-to-chaos transition is a rather smooth affair: Perturbations of an integrable hamiltonian usually do not immediately bring the system to a completely chaotic regime, but make it pass some transitional region. The explanation of this behaviour in the classical case was the main goal of the famous KAM theorem [1]. However, what *in the dynamical-symmetry language* controls the degree of quantum chaos?

In this paper we would like to show that not only the degree of chaos inherent in the system, but also its “dynamical-symmetry content” can be measured by a continuous quantity. Our approach is based on the fact that any particular dynamical symmetry is associated with a certain basis (or a subclass of bases in general). This basis, obtained by the simultaneous diagonalization of Casimir operators of all groups in the dynamical-symmetry chain, becomes a reference frame in the system’s Hilbert space. The degree of localization of actual eigenstates in the reference basis, i.e., the degree of overlap of the two bases then represents

the desired continuous measure which tells us “how close” to the given integrable case the actual system is. In this logic, chaos is smoothly established as the degree of eigenstate localization in the bases corresponding to all possible dynamical-symmetries of the system decreases.

To illustrate these general ideas, we invoke the simplest version (IBM-1) of the Interacting Boson Model [12], which is known to efficiently describe basic aspects of collective motion in atomic nuclei. Apart from the advantage that the IBM group structure is explicitly known, the model also sets a field for practical applications of our investigations in realistic systems. To quantify the eigenstate localization of a particular transitional IBM-1 hamiltonian in a given dynamical-symmetry basis, we use the so-called information entropy of wave functions. It will be shown that the entropy analysis of eigenfunctions enables one to find a counterpart of all order/chaos properties of the IBM-1 in terms of the known dynamical symmetries associated with this model.

Here is the plan of the paper: Properties of the particular form of the IBM-1 used are discussed in Sect.II, while general features of the wave-function entropy are described in Sect.III. In Sect.IV, we present results of the entropy calculations for various transitional IBM-1 hamiltonians in dependence on the angular momentum and boson number, and show their relation to the chaotic properties of the model. Sect.V brings a few concluding remarks.

## **II. MODEL**

### **A. Dynamical group**

As already indicated above, in this work we will study the wave-function entropy within the Interacting Boson Model–1. The IBM-1 was introduced in 1974 by Arima and Iachello with the aim to describe collective nuclear excitations in an algebraic framework (see references in Refs. [6,12]) and has soon since evolved into more sophisticated and powerful boson models [6]. Because we do not make a specific link to nuclear physics here (although some

of the results may turn out applicable there), we use the original and simplest version of the IBM.

The IBM-1 is formulated as a model describing one- and two-body interactions of two kinds of bosons, named s- and d-bosons according to their spins  $l=0$  and 2, respectively. Because the interactions conserve the total number of bosons  $N$ , the dynamical group of the model is the  $U(6)$  generated by the 36 bilinear products of the boson creation and annihilation operators:  $s^\dagger s$ ,  $d_m^\dagger d_{m'}$ ,  $d_m^\dagger s$  and  $s^\dagger d_m$  ( $m, m' = -2 \dots +2$ ). The hamiltonian, built only from these products, is further made invariant under time reversal and rotations by allowing for only the hermitian terms with zero total angular momentum. Carrier spaces of irreducible representations of the dynamical group, each of them corresponding to a fixed boson number  $N$ , naturally coincide with possible quantum Hilbert spaces ascribed to the model. If the boson operators in the IBM-1 hamiltonian are rewritten in a convenient coordinate representation, the model turns out to describe rotations and quadrupole vibrations of a specific quantum “drop”.

## B. Dynamical symmetries and integrability

Possible dynamical symmetries of the IBM-1 are found by constructing various subgroup chains of the dynamical group  $U(6)$ , all ending at the angular-momentum group  $SO(3)$  generated by the products  $[d^\dagger \times \tilde{d}]_\mu^{(1)}$  (standard definitions  $[b_l^\dagger \times \tilde{b}_{l'}]_\mu^{(\lambda)} = \sum_{mm'} (lm l' m' | \lambda \mu) b_{lm}^\dagger \tilde{b}_{l' m'}$  and  $\tilde{b}_{lm} = (-1)^{l+m} b_{l-m}$  are used), which must remain the symmetry group of the hamiltonian. Such, one finds the following three chains [6,12]:

$$\begin{aligned}
 \text{(I)} \quad & U(6) \supset U(5) \supset SO(5) \supset SO(3) , \\
 \text{(II)} \quad & U(6) \supset SU(3) \supset SO(3) , \\
 \text{(III)} \quad & U(6) \supset SO(6) \supset SO(5) \supset SO(3) .
 \end{aligned}
 \tag{2}$$

Note that the concrete realization of some groups in (2) is not unique because of phase ambiguities of the boson operators. We will come to that point later.

A possible set of Casimir operators  $\hat{\mathcal{C}}_i[\text{G}]$  of the first and/or second order ( $i=1$  and/or 2, respectively) of the groups G involved in the chains (2) is listed in Tab.I (dots denote the scalar product defined by  $A^{(\lambda)} \cdot B^{(\lambda)} = \sum_{\mu} (-1)^{\mu} A_{\mu}^{(\lambda)} B_{-\mu}^{(\lambda)}$ ). The U(6) invariants were skipped because, as already mentioned above, within the IBM-1 one always takes into account only one finite-dimensional subspace of the total Hilbert space corresponding to a fixed (sharp) boson number  $N$ , where the U(6) Casimir operators yield just ordinary numbers. The most general IBM-1 hamiltonian can be written as a linear superposition (weighted sum) of the invariants from Tab.I and, as such, it has 6 free parameters — the weights. If all the weights are zero except for those standing at invariants of only one group chain in (2), the hamiltonian has the dynamical symmetry described by the given chain. Hereafter, we will distinguish these dynamical symmetries by the name of the corresponding largest subgroup, i.e., by labels U(5), SU(3) or SO(6), respectively. These limits correspond to vibrational, rotational and  $\gamma$ -unstable nuclei [6,12].

The above-specified symmetries do not, however, exhaust all possible dynamical symmetries of the model. Namely, phase ambiguities in the definition of boson operators lead to two additional symmetries connected with the following chains [6,12–15]:

$$\begin{aligned} \text{(II)*} \quad & \text{U(6)} \supset \text{SU(3)*} \supset \text{SO(3)} , \\ \text{(III)*} \quad & \text{U(6)} \supset \text{SO(6)*} \supset \text{SO(5)} \supset \text{SO(3)} . \end{aligned} \tag{3}$$

The group SU(3)\* is made from the “standard” SU(3) by the transition  $(d_m^{\dagger}, \tilde{d}_m) \rightarrow (-d_m^{\dagger}, -\tilde{d}_m)$  (which is equivalent to taking  $\chi = +\sqrt{7}/2$  instead of  $-\sqrt{7}/2$  in  $\hat{\mathcal{C}}_2[\text{SU(3)}]$ , see Tab.I) and SO(6)\* is made from SO(6) by  $(d_m^{\dagger}, \tilde{d}_m) \rightarrow (-id_m^{\dagger}, i\tilde{d}_m)$  (equivalent to  $\phi=0$  instead of  $\pi$  in  $\hat{\mathcal{C}}_2[\text{SO(6)}]$ ). The SU(3)\* and SO(6)\* Casimir operators can be written as linear superpositions of the Casimir operators in Tab.I [15]. Therefore, the hamiltonian has dynamical symmetry SU(3)\* (II\*) or SO(6)\* (III\*) if some of the weights in its expansion have certain ratios. In particular [15], the SU(3)\* dynamical symmetry sets in if ratios of the coefficients at Casimir operators (see Tab.I)  $\hat{\mathcal{C}}_1[\text{U(5)}]$ ,  $\hat{\mathcal{C}}_2[\text{U(5)}]$ ,  $\hat{\mathcal{C}}_2[\text{SO(6)}]$ ,  $\hat{\mathcal{C}}_2[\text{SO(5)}]$ , and  $\hat{\mathcal{C}}_2[\text{SU(3)}]$  are  $2 : 2 : 4 : -6 : -1$ , whereas the SO(6)\* dynamical symmetry requires the

ratios  $4(N + 2) : -4 : -1 : \text{arbitrary} : 0$ .

Since all phase conventions must fulfil restrictions following from rotational and time-reversal invariance of the resulting hamiltonian, the above five chains most probably represent a complete set of the IBM-1 exact dynamical symmetries. This is not so, however, as far as the integrability of the model is concerned. The IBM-1 is, in fact, a straightforward example showing that although a dynamical symmetry really implies integrability, the opposite implication (proposed in Ref. [9] but soon abandoned [11]) does not, in general, hold. To see that, consider the IBM-1 hamiltonian which is transitional between the U(5) and SO(6) dynamical symmetries, but has no admixture of the SU(3) invariant. Neither the U(5) nor the SO(6) invariant is an integral of motion on the U(5)–SO(6) transition, but the hamiltonian itself, which is always a trivial commuting integral of motion, becomes independent from the other integrals, which ensures that the integrability is preserved if the SO(5)-generated dynamical symmetry is taken into account [16,17]. This is a special case of the self-evident rule that non-integrability does not appear if the dynamical-symmetry breaking destroys just one integral of motion [11]. For instance, if apart from the chain (1) also  $G \supset G_1 \supset \dots \supset G'_i \supset \dots \supset G_k$  (differing only by the  $i$ -th subgroup) is a valid group reduction, the transition between these two dynamical symmetries is always totally integrable, although having no dynamical symmetry in the above sense.

### C. Casten triangle

The six free parameters of the most general IBM-1 hamiltonian is a too large number if features of the model are to be systematically scanned over the whole parameter space. Nevertheless, it is often enough to select a certain subset of hamiltonians out of the complete set generated by the dynamical group. Usually a two-dimensional manifold is spread in the six-dimensional parameter space so that the U(5), SU(3), and SO(6) limits are reached for some particular points. The manifold is then mapped onto the so-called Casten triangle, whose vertices correspond to these limits.

Chaotic properties of a specific two-parameter set of IBM-1 hamiltonians were throughoutly studied by Alhassid, Whelan, and Novoselsky [16–20]. As we follow the cited works in order to relate the order/chaos signatures to the dynamical-symmetry content, we use the same parameterization of the IBM-1 hamiltonian. It is given by the following formula (see Tab. I):

$$\hat{H}_{(N,\eta,\chi)} = \eta \hat{n}_d - \frac{1-\eta}{N} \hat{Q}_\chi \cdot \hat{Q}_\chi . \quad (4)$$

Here, two control parameters  $\eta$  and  $\chi$  change within the bounds  $0 \leq \eta \leq 1$  and  $-\sqrt{7}/2 \leq \chi \leq 0$ . If  $\eta=1$ , the hamiltonian (4) has the U(5) symmetry, while with  $\eta=0$  the hamiltonian has the SU(3) symmetry for  $\chi=-\sqrt{7}/2$  or the SO(6) symmetry for  $\chi=0$ . For other parameter values, the hamiltonian has no dynamical symmetry, i.e., is transitional between two or more limits.

The statements concluding the last paragraph can be particularly easily read in the following expansion of Eq. (4) into Casimir operators from Tab. I:

$$\begin{aligned} \hat{H}_{(N,\eta,\chi)} = & \left[ \eta - \frac{1-\eta}{N} \left( \frac{\chi}{\sqrt{7}} + \frac{2\chi^2}{7} \right) \right] \hat{C}_1[\text{U}(5)] - \frac{1-\eta}{N} \left( \frac{\chi}{\sqrt{7}} + \frac{2\chi^2}{7} \right) \hat{C}_2[\text{U}(5)] - \\ & - \frac{1-\eta}{N} \left( 1 + \frac{2\chi}{\sqrt{7}} \right) \hat{C}_2[\text{SO}(6)] + \frac{1-\eta}{N} \left( 1 + \frac{3\chi}{\sqrt{7}} + \frac{2\chi^2}{7} \right) \hat{C}_2[\text{SO}(5)] + \\ & + \frac{1-\eta}{N} \frac{\chi}{\sqrt{7}} \hat{C}_2[\text{SU}(3)] - \frac{1-\eta}{N} \left( \frac{\chi}{\sqrt{7}} + \frac{\chi^2}{14} \right) \hat{C}_2[\text{SO}(3)] . \end{aligned} \quad (5)$$

What we further see from this expansion is that while the hamiltonians with  $\chi=0$  or  $\chi=-\sqrt{7}/2$  ( $\eta$  varying) are purely U(5)–SO(6) or U(5)–SU(3) transitional, respectively (they contain no admixture of the SU(3) or SO(6) Casimir operators, respectively), the  $\eta=0$  ( $\chi$  varying) case represents the SU(3)–SO(6) transition with some amount of the U(5) “impurity” (see a schematic illustration in Fig. 1).

The hamiltonian (4)=(5) reaches neither the SU(3)\* nor the SO(6)\* symmetry for any values ( $\eta, \chi$ ) [15]. However, one could easily write another two-dimensional parameterization that would pass the SU(3)\* and/or SO(6)\* dynamical symmetries somewhere in the middle of the Casten triangle (more precisely, the SU(3)\* can indeed lie in the middle, but the



$SO(6)^*$  can only be on the  $U(5)$ – $SO(6)$  edge [14,15]). One therefore has to be very careful in generalizing results obtained within a single parameterization. If, as an example, the  $SU(3)^*$  and/or  $SO(6)^*$  dynamical symmetries are, in the special parameterization, reached for some intermediate values of the control parameters, the hamiltonian would unexpectedly receive quite regular properties in a seemingly transitional region. This behaviour, however, would never be encountered in an ordinary parameterization.

We conclude this section with a few remarks on the classical analogue of the quantal hamiltonian (4). As argued in Refs. [19,17], the on the first view incomprehensible factor  $1/N$  in Eq. (4) is a consequence of the quantum–classical correspondence. The dynamics of the IBM-1 classical counterpart is reached for  $N \rightarrow \infty$  (for instance, coherent states stop overlapping in this limit) after appropriate rescaling of the dynamical variables and hamiltonian parameters. It is clear that matrix elements of the quadratic Casimir invariants (having the  $\mathcal{O}(N^2)$  behaviour) completely dominate the ones of linear invariants ( $\sim \mathcal{O}(N)$ ) in the  $N \rightarrow \infty$  limit, which means that quantum IBM-1 hamiltonians differing only in linear terms have all the same classical analogue. This common ambiguity of the quantum-to-classical transition would be very unpleasant here, because for chaos the classical behaviour is constituent. Fortunately, the difficulty can be bypassed by the  $1/N$  damping of the quadratic terms. In fact, such modified hamiltonian is not a “textbook” IBM-1 hamiltonian (it would contain the uneasy operator  $1/\hat{N}$  if acting in the general Fock space), but it does not matter in our case since  $N$  has always a sharp value. In this modified model, the sets of eigenvalues and corresponding eigenvectors for various  $N$  determine quantum aspects of classically the same system, similarly as the 3D-oscillator states with finite quantum numbers  $N$  ( $= n_x + n_y + n_z$ ) all issue from the unique classical origin (which the quantum system imitates in the  $N \rightarrow \infty$  limit).

Following the procedure described in Ref. [19], one derives the classical hamiltonian  $H(p_i, q_i)$  (with  $i=1 \dots 5$ ) corresponding to Eq. (4). The coordinates  $q_i$  can be identified with the quadrupole-shape variables  $\beta, \gamma$  and Euler angles, known from the nuclear liquid-drop model, and  $p_i$  are associated momenta. The classical potential, i.e., the function  $H(p_i=0, q_i)$ ,

looks as follows (cf. Ref. [21]):

$$V_{(\eta,\chi)}(\beta, \gamma) = \left[ \frac{5}{2}\eta - 2 \right] \beta^2 + \left[ (1 - \eta) \left( 1 - \frac{\chi^2}{14} \right) \right] \beta^4 + \left[ \frac{2}{\sqrt{7}}(1 - \eta)\chi \right] \beta^3 \sqrt{1 - \frac{\beta^2}{2}} \cos(3\gamma) . \quad (6)$$

This function is shown, for some particular  $(\eta, \chi)$  values, in Fig. 2. In agreement with a general rule, one sees that the U(5), SU(3) and SO(6) limits correspond to, respectively, spherical ( $\beta=0$ ,  $\gamma$  arbitrary), deformed axially symmetric ( $\beta \neq 0$ ,  $\gamma=0$ ) and deformed “ $\gamma$ -soft” ( $\beta \neq 0$ ,  $\gamma$  arbitrary) shapes at the minimum potential energy. A “phase transition” [12] from deformed to spherical shape can be observed for  $\eta=4/5$ , where the potential develops a minimum at  $\beta=0$ . Although all features of the IBM-1 classical limit certainly cannot be derived from the potential alone (kinetic terms of the Hamilton function also have a rather specific form), the  $\eta=4/5$  value can be, within some plausible simplification, seen as a border between various classical modes of the model (a more sophisticated approach was recently described in Ref. [22]).

### III. WAVE-FUNCTION ENTROPY

#### A. Definition

The Shannon information entropy of wave functions [23–29,15] is a natural measure of the localization of wave functions in a given basis. The wave-function entropy (as we will briefly call it) of a state  $|\psi\rangle$  with respect to the basis  $\mathcal{B} \equiv \{|i^{\mathcal{B}}\rangle\}_{i=1}^n$  ( $n$  is the dimension of the Hilbert space) is defined by the following formula:

$$W_{\psi}^{\mathcal{B}} = - \sum_{i=1}^n |a_{\psi i}^{\mathcal{B}}|^2 \ln |a_{\psi i}^{\mathcal{B}}|^2 , \quad a_{\psi i}^{\mathcal{B}} = \langle i^{\mathcal{B}} | \psi \rangle . \quad (7)$$

It is minimum ( $W_{\psi}^{\mathcal{B}} = 0$ ) if  $|\psi\rangle$  coincides with one of the basis vectors, while the maximum ( $W_{\psi}^{\mathcal{B}} = \ln n$ ) is reached if  $|\psi\rangle$  is spread uniformly among all basis states, i.e., if  $|a_{\psi i}^{\mathcal{B}}|^2 = 1/n$ . The intermediate entropy values indicate a partial fragmentation of the state  $|\psi\rangle$  in the basis  $\mathcal{B}$ .

## B. Reference bases

An apparent question accompanying the use of the wave-function entropy concerns an appropriate selection of the reference basis. Of course, this selection must issue from the physical aims followed. If effects of some perturbation on the system are to be measured, the reference basis will naturally be the eigenbasis of the unperturbed hamiltonian. Recent studies of Zelevinsky *et al.* [29–32] provide an interesting example. In these works, the *sd*-shell model with residual two-body interactions was considered, and “dissolving” of the actual eigenstates in the shell-model basis was measured for a system of 12 fermions. It was shown that for realistic strengths of residual interactions the relative wave-function entropy of individual states along the spectrum follows almost exactly the state-density logarithm, which allows one to relate the wave-function and thermodynamic entropies. For bases unrelated to the unperturbed hamiltonian, however, the entropy was equally large for all states (just like in the case of too strong residual interactions) indicating the irrelevance of the basis selected.

In our case, selection of the reference bases naturally follows from the demand to measure a “similarity” of a given general hamiltonian to the dynamical-symmetry limits. Associated with each integrable (dynamically symmetric) system is a set of mutually commuting integrals of motion, which (in a favourable case) defines a single physically important basis or (in general) a subclass of bases. The basis is not always unique because the system can allow for building more independent sets of integrals of motion. The IBM-1 is a good example: In this case, the dynamical-symmetries contain some missing labels [6,12], which means that Casimir operators of any given chain must be supplied by some other operators to form a complete set of commuting integrals of motion [9,11]. For various choices of the additional commuting operators one obtains generally different bases. All these are eigenbases of the corresponding dynamical-symmetry hamiltonian, and the ambiguity of the basis selection can be seen as resulting from unavoidable spectral degeneracies in the IBM-1 limits due to the missing labels. Nevertheless, we will see later that in the cases studied these am-

biguities are not large enough to paralyze predictions based on a particular choice of the dynamical-symmetry basis.

It must be emphasized that the constraints on the basis in the Hilbert space are the only signatures of a particular dynamical symmetry (or a particular case of integrability). Indeed, as can be easily evidenced, the spectrum corresponding to an integrable system can be made arbitrary without changing integrals of motion (i.e., preserving the integrability) if only the eigenbasis is conserved. Also any given dynamical symmetry can be associated with an arbitrary spectrum since the symmetry itself does not impose any constraints upon the way in which the hamiltonian depends on the associated Casimir invariants. A  $U(6)$ -generated boson hamiltonian, for instance, with a given dynamical symmetry does not have to follow the special form assumed in the IBM-1, but could be an arbitrary function of general-order Casimir operators of the given group chain. The non-generic spectral properties of various integrable systems, such as the non-Poissonian level spacing distribution recently noticed [33] and explained [34] in the IBM-1 for a particular  $SU(3)$  hamiltonian, e.g., seem to illustrate these matters.

In this work, we use the wave-function entropy to quantify the departure of transitional IBM-1 hamiltonians in Eq. (4) from the particular dynamical symmetries of the model. The bases  $\mathcal{B}$  of interest will thus be associated with the limits (2) and (3) and we will deal with  $\mathcal{B} \equiv U(5)$ ,  $SU(3)$ ,  $SO(6)$ ,  $SU(3)^*$ , and  $SO(6)^*$  entropies. As pointed out above, the IBM-1 dynamical-symmetry bases are not unique due to the degeneracy caused by missing labels, which is a problem that must be solved first. To do it precisely, one should evaluate each of the above five entropies in all bases allowed by the respective symmetry and discuss results with regard to the obtained uncertainty intervals. Nevertheless, it can be directly shown that the uncertainties should not be very large in the cases studied because of a relatively low average multiplicity of degeneracies. In fact, one has to consider what amount of the wave-function amplitudes in a given dynamical-symmetry basis remains uncertain due to the basis ambiguity. If 100% is assigned to a completely degenerated hamiltonian and 0 to a quite non-degenerated one, the following quantity can be used to measure this amount:

$$f_{\text{deg}} = \frac{\sum_i n_{\text{deg}}^{(i)} (n_{\text{deg}}^{(i)} - 1)}{n(n-1)}. \quad (8)$$

Here,  $n_{\text{deg}}^{(i)}$  is the dimension of the  $i$ -th degenerated subspace and  $n$  is the total dimension. The values of  $f_{\text{deg}}$  for various angular-momentum ( $L$ ) subspaces and various boson numbers ( $N$ ) are shown in Tab. II. Note that we have in mind here only the inherent degeneracy due to missing labels, not accidental degeneracies resulting from a special form of the hamiltonian, such as the degeneracy caused by the absence of the SO(5) and SO(3) terms in the U(5) limit of Eq. (4). It is evident from Tab. II that even in the SU(3) and SU(3)\* limits, which are most degenerated, the uncertainty is still relatively small. We therefore do not proceed in the above-proposed accurate way, but select a single basis for each limit. Namely, for evaluating the U(5) entropy we used the standard basis  $\{|[N]n_d v n_\Delta L\rangle\}$  [6,12], while bases for the other limits were determined by a numerical diagonalization of the respective hamiltonian matrices in the standard U(5) representation (which means that the bases  $\mathcal{B} \neq \text{U}(5)$  were not the standard ones).

### C. Average entropy

To measure the dynamical-symmetry content of a given transitional IBM-1 hamiltonian  $\hat{H}_{(N,\eta,\chi)}$ , we will average the wave-function entropy defined in Eq. (7) over all eigenstates  $\{|\alpha, L\rangle_{(N,\eta,\chi)}\}_{\alpha=1}^{n(L,N)}$  (with fixed angular momentum  $L$ ) of  $\hat{H}_{(N,\eta,\chi)}$ :

$$W^{\mathcal{B}}(L, N, \eta, \chi) \equiv W^{\mathcal{B}} = \frac{1}{n(L, N)} \sum_{\alpha=1}^{n(L, N)} W_{\alpha}^{\mathcal{B}}(L, N, \eta, \chi) \quad (9)$$

Here,  $W_{\alpha}^{\mathcal{B}}(L, N, \eta, \chi)$  is the single-state wave-function entropy of  $|\alpha, L\rangle_{(N,\eta,\chi)}$ . The average entropy  $W^{\mathcal{B}}$  expresses how much the whole eigenbasis (for the fixed  $L$ ) of the hamiltonian under study overlaps with the given dynamical-symmetry reference basis.

Note that now the problem with degeneracies reappears. This time it does not concern the reference hamiltonians, but the tested hamiltonian  $\hat{H}_{(N,\eta,\chi)}$  which is at some values of  $\eta$  and  $\chi$  also degenerated, leaving the corresponding average entropy uncertain. However, in

the cases studied this uncertainty must undoubtedly be very small, and we will neglect it in the following.

More serious is another problem: To enable one to compare average entropies of eigenvector sets with various dimensions  $n(L, N)$ , it is necessary to develop a proper normalization. As we already pointed out, the maximum entropy of a single state in an  $n$ -dimensional Hilbert space is  $\ln n$ . For  $n=2$ , this entropy is shared by both eigenvectors of a non-diagonal hamiltonian in case of the maximum mixing (equal diagonal elements of the hamiltonian). For  $n > 2$ , however, the entropy of a set of hamiltonian eigenstates is influenced by the orthogonality constraints. To calculate the maximum average wave-function entropy for  $n > 2$  orthonormal states becomes tricky, but there is no doubt that the result is smaller than  $\ln n$  and depends on  $n$ .

We solve the above problem by adopting the approach of random-matrix theory [3]. The idea is to take a set of  $n$  fixed orthonormal vectors in the  $n$ -dimensional space and to expand them in various orthonormal bases, created by random rotations of the initial frame. The resulting distribution of the average entropy  $W$  depends on  $n$  and its average, for instance, may provide the desired normalization quantity. This procedure can be easily realized with the Gaussian Orthogonal Ensembles (GOE) [3]. By randomly generating  $n$ -dimensional matrices with the GOE constraints, the above distribution is obtained from values of  $W$  assigned to the set of  $n$  orthonormal eigenvectors.

For large dimensions  $n$ , the GOE average  $\langle W \rangle_{\text{GOE}n}$  of the entropy  $W$  can be expressed explicitly:

$$\langle W \rangle_{\text{GOE}n} \approx -\sqrt{\frac{2n^3}{\pi}} \int_0^1 x^2 \ln(x^2) \exp\left(-\frac{nx^2}{2}\right) dx \approx \ln(0.482n) \quad (10)$$

(see also Ref. [32]). For small  $n$ , however, serious deviations from this value can be expected due to non-Gaussian distributions of the eigenvector components. We performed a Monte-Carlo simulation whose results are shown in Fig.3. The ensemble average  $\langle W \rangle_{\text{GOE}n}$  and the band which contains 90% of the  $W$  distribution are both shown in Fig.3a for dimensions  $n=2-30$ . As can be seen,  $\langle W \rangle_{\text{GOE}n}$  is considerably lower than  $\ln n$ . The width of the entropy

distribution decreases with  $n$ , which is demonstrated also by the relative r.m.s. deviation  $d$  of the entropy  $W$  from the GOE average in Fig.3b. In Fig.3b, in addition, the coefficient  $\alpha_n$  from a parameterization  $\langle W \rangle_{\text{GOE}n} = \ln(\alpha_n n)$  is displayed. The convergence of  $\alpha_n$  to its asymptotic value from Eq.(10) is evident.

For any set of  $n$  orthonormal vectors, the average entropy  $W^{\mathcal{B}}$  in a *randomly chosen* basis  $\mathcal{B}$  will most probably be close to  $\langle W \rangle_{\text{GOE}n}$  (cf. [29–32]). It is therefore reasonable to normalize the entropy values to the GOE average. We emphasize, however, that the fraction  $W^{\mathcal{B}}/\langle W \rangle_{\text{GOE}n}$  can be even larger than 1. To be absolutely exact, one should take into account also the fact that the range of probable deviations of the GOE-normalized entropy from unity depends on  $n$  since the shapes of the entropy distribution for various dimensions differ. The deviations can be characterized by the probability localized below (or above)  $W^{\mathcal{B}}$  (see, for instance, the lower and upper 5% limits displayed in Fig.3a as the “GOE 90%” band). Therefore, the GOE distributions of the wave-function entropy can, in principle, induce a kind of metric for measuring the proximity of a given basis to another one.

#### D. Entropy-ratio product

In the following, we will most often display the entropy ratio [15]

$$r^{\mathcal{B}} = \frac{\exp W^{\mathcal{B}} - 1}{\exp \langle W \rangle_{\text{GOE}n} - 1} . \quad (11)$$

Note that the quantity  $n_{\text{eff}\psi}^{\mathcal{B}} = \exp W_{\psi}^{\mathcal{B}}$  can be understood as an effective number of wave-function components of the state  $|\psi\rangle$  in the basis  $\mathcal{B}$  (it changes between 1 and  $n$ ). An analogous quantity,  $n_{\text{eff}}^{\mathcal{B}} = \exp W^{\mathcal{B}}$ , derived from the average entropy is some “average” (not the rigorous statistical average) effective number of wave-function components assigned to a given eigenvector set. The fraction  $\exp W^{\mathcal{B}}/\exp \langle W \rangle_{\text{GOE}n} = n_{\text{eff}}^{\mathcal{B}}/\alpha_n n$  has a better “contrast” than the GOE-normalized entropy  $W^{\mathcal{B}}/\langle W \rangle_{\text{GOE}n}$ , but its lower bound depends on  $n$ . The quantity in Eq.(11) has both a good contrast and a constant (=0) lower bound.

To express simultaneously the average overlap of a given eigenbasis with all the reference bases, we introduce the product of the five entropy ratios from Eq. (11):

$$R = C \prod_{\mathcal{B}=\text{U}(5)\dots\text{SO}(6)^*} r^{\mathcal{B}}, \quad (12)$$

where  $C$  is an arbitrary normalization constant. Trivially,  $R$  is zero if any of the ratios  $r^{\mathcal{B}}$  vanishes, while if all  $r^{\mathcal{B}}$ s are large ( $\approx 1$ ),  $R$  is large, as well. This qualifies the entropy-ratio product  $R$  to decide whether the system is close (or not) to any of the five possible dynamical symmetries regardless of what symmetry it actually is. However, the reasoning is not as clear if  $R$  is small due to a simultaneous partial suppression of more ratios  $r^{\mathcal{B}}$  in Eq. (12). Then a question raises, whether the partial influence of several individual symmetries on the system's behaviour is really "cumulative" in such a case (as implicitly assumed in the construction of  $R$ ) or whether one should not take into account only the nearest symmetry (i.e., to use the minimum of the five ratios  $r^{\mathcal{B}}$  instead of  $R$ ). Based on a good correlation of the product  $R$  with standard chaotic measures, as it will be presented below, we incline to believe that its definition is justified.

#### IV. RESULTS

In their remarkable series of works [18,16,19,20,17], Alhassid, Whelan, and Novoselsky mapped the classical and quantum signatures of chaos associated with the hamiltonian (4) in the whole  $(\eta,\chi)$ -parameter range for various angular momenta. As shown in a recent work [15], the observed behaviour of standard chaotic measures has a counterpart in the behaviour of the entropy-ratio product  $R$  from Eq.(12). We review these results in more detail (paragraphs C and D below) and discuss (par. E) also the role of the boson number  $N$ . Before (par. A, B) we concentrate on properties of the wave-function entropy of individual states in some less complex cases.



### A. U(5)-symmetry breaking

If the value of  $\eta$  goes down from 1, the hamiltonian (4) loses the U(5) dynamical symmetry. As shown in Sect. II, the  $\beta=0$  minimum of the potential (6), characteristic for the U(5) limit ( $\eta=1$ ), keeps existing to the limiting value  $\eta=4/5$ , where a “phase transition” to a deformed shape takes place in the classical system. It is therefore interesting to look at what happens around this critical value with the quantum system. In the quantum case, the U(5)-symmetry breaking can be monitored by the wave-function entropy, which is clearly zero at the U(5) vertex, but increases as the symmetry is being departed. The average U(5) entropy — or, more precisely, the ratio  $r^{\text{U}(5)}$  from Eq. (11) — of all states with angular momentum  $L=0$  is shown for the U(5) side of the Casten triangle, namely for  $0.5 \leq \eta \leq 1$ , in the left column of Fig. 4. The two histograms correspond to boson numbers  $N=10$  and  $N=20$  (in both cases, the number  $n$  of  $L=0$  states is indicated).

The average spread of the actual eigenstates in the U(5) basis, as shown in the left column of Fig. 4, changes quite smoothly — no abrupt transition appears neither at  $\eta=4/5$  nor at any other value. However, it is not quite so if the ground state alone is concerned. The ground state is, of course, most sensitive to changes of the potential minimum. Indeed, the ground-state’s U(5)-entropy ratio  $r_1^{\text{U}(5)}$ , shown in the middle two histograms in Fig. 4., changes rapidly around the critical  $\eta$  value. The squared amplitude modulus corresponding to the admixture of the unperturbed U(5) ground state in the actual ground state is displayed in the right-hand column of Fig. 4. It is evident that changes of the ground state become, in agreement with general expectations [7,12], sharper as the boson number  $N$  increases. These results might turn out interesting in connection with a recent attempt to attribute a critical phase-transitional behaviour (rotor–vibrator) to low-lying collective states in atomic nuclei [35].

## B. U(5)–SU(3) transition

The IBM-1 enables one to study not only processes of a single-symmetry breaking, but also transitions between two or more symmetries. The entropy measures connected with both the dynamical-symmetry bases in play then quantify breaking of one symmetry and the simultaneous onset of a new symmetry. Here we consider the transition between U(5) and SU(3) limits of the hamiltonian in Eq. (4), namely the way from  $\eta=1$  to  $\eta=0$  along the  $\chi=-\sqrt{7}/2$  edge of the Casten triangle (see Fig. 1). The U(5) and SU(3) wave-function entropies for individual  $L=10$  states with  $N=20$  are shown in Fig. 5 (notice that the orientation of axes is opposite in both histograms). In accord with the previous paragraph, an average of the single-state entropies gradually increases as the respective dynamical symmetry is left. However, the histograms in Fig. 5 show in more detail the way in which the symmetry breakdown proceeds: The variable  $\alpha = 1 \dots 121 (=n)$  enumerates the eigenstates  $|\alpha, L\rangle_{(N,\eta,\chi)}$  consecutively with the increasing energy. When departing from a given symmetry, the mixing of states concerns at first more the medium-energy states than the states on the spectral tails. This is still valid somewhere on the midway between the two symmetries. Nevertheless, the respective entropies keep growing until a saturation value, roughly equal to the GOE average, is reached for almost all states except for a few ones on the tails.

This behaviour can be related to general trends following from perturbation theory. Eigenstates of a hamiltonian affected by a small perturbation are mixtures of unperturbed eigenstates. The amplitude of the  $j$ -th unperturbed state (with energy  $E_j$ ) in the  $i$ -th perturbed state (whose unperturbed energy was  $E_i$ ) is proportional to  $1/|E_i - E_j|$  times the mixing matrix element. The eigenstate density culminates (for models with finite state numbers) in the middle of the spectrum, which means that in the statistical case (“random” matrix elements of the perturbation) the mixing should be maximal there, as well. When the perturbation strength becomes large enough to mix states from opposite ends of the spectrum, practically all wave functions reach the GOE entropy value.

As already discussed in Sect. IIIB, such scenario seems to work also in the shell model

[29–32]. However, it must be stressed that it can be invalid in some cases, especially if there exist some “non-statistical” structural effects along the spectrum, as illustrated in the following example: Consider two classes of the IBM-1 states, both being mixtures of the U(5) eigenstates with various d-boson numbers. Let  $n_d \leq n_{d0}$  for the first class of states and  $n_d > n_{d0} + 2$  for the second class ( $n_{d0}$  is an arbitrary number smaller than  $N-2$ ). The states from both classes cannot be mixed by a two-body interaction, so that if they prevail in some part of the spectrum, the wave-function entropy would be systematically reduced there compared to the level-density expectation.

We should have in mind that in our case the above-discussed correspondence between the complexity and density of eigenstates must be imperfect since the changes of the IBM-1 hamiltonian under study are not small perturbations. The  $\eta$ -dependence of a smoothed state density

$$\rho(E) = \int \rho_e(E') g(E - E') dE' , \quad (13)$$

where  $\rho_e(E)$  is the exact state density (a chain of delta-functions) and  $g(E - E')$  is an appropriate zero-centered gaussian ( $\sigma=0.07$  energy units), is shown in the upper part of Fig. 6. Apparently, the level distribution moves as a whole and changes in shape under the U(5)→SU(3) transition (cf. the corresponding change of the potential in Fig. 2). Thus the behaviour of wave-function entropies in Fig. 5 can be even surprising. Anyway, no wonder that, unlike the shell-model case [29–32], the entropies in Fig. 5 cannot be directly related to the “thermodynamic entropy” given by a logarithm of the state density. This can be seen by comparing the histograms in Fig. 5 with the one in the lower part of Fig. 6, where the smoothed state density  $\rho(E_\alpha)$  is shown as a function of the state index  $\alpha$  (considering the different orientations of the plots in Fig. 5 and 6, imposed by the shape of the functions displayed). Clearly,  $\rho(E_\alpha)$  does not exactly correspond to  $\exp W_\alpha^B$ . Note, however, that dimensions  $n$  in the present model are still too low to make a definite conclusion in this question.

### C. U(5)–SU(3)–SO(6) transitions

The average wave-function entropy in the whole  $(\eta, \chi)$ -range of Eq. (4) with  $N=20$  was presented in our previous work [15] for various angular momenta. It was shown that the regions with largest entropy-ratio product  $R$  from Eq. (12) coincide with the most chaotic regions of the Casten triangle described in Refs. [16,17] by standard quantal and classical chaotic measures. On the other hand, the semiregular regions have the  $R$ -product suppressed.

An example is in Fig. 7, where the average-entropy ratios  $r^B$  are shown for all five symmetries together with the product  $R$  for  $L=10$  states with  $N=20$  (cf. Fig. 1 in Ref. [15]). Note that because the non-standard symmetries  $SU(3)^*$  and  $SO(6)^*$  are absent from the  $(\eta, \chi)$ -manifold in the present parameterization, the corresponding entropies are never zero. However, while the  $SU(3)^*$  symmetry is totally irrelevant (it would be present if the triangle is extended to  $\chi=+\sqrt{7}/2$ ), the  $SO(6)^*$  entropy has a behaviour very similar to  $U(5)$ .

One sees in Fig. 7 that the regular region at the  $U(5)$ – $SO(6)$  edge [16,17,36] exhibits a quite high simultaneous localization in the  $U(5)$ ,  $SO(6)$  and  $SO(6)^*$  bases. This is because *the same*  $SO(5)$  subgroup is common to all the three chains I, III and III\*, see (2) and (3), so that the  $\chi=0$  hamiltonians cannot mix states with various  $SO(5)$ -associated quantum numbers. The block-diagonal form of the hamiltonian then naturally implies the suppression of the above three entropies and also non-GOE spectral characteristics [36] on the  $U(5)$ – $SO(6)$  transition. As was already discussed, however, the system not only exhibits a smaller degree of chaos but is fully integrable in this region, since, having five degrees of freedom (for a fixed  $N$ ; see Sect. II C), it also has five independent compatible integrals of motion (if not counting  $\hat{N}$ ):  $\hat{C}_2[SO(5)]$ ,  $\hat{L}^2$ ,  $\hat{L}_z$ , the integral associated with the missing label in the  $SO(5) \supset SO(3)$  embedding (an invariant of  $SO(3)$  built from the  $SO(5)$  generators), and the hamiltonian itself [16,17].

Note that we reveal the integrable  $U(5)$ – $SO(6)$  region using only the bases associated with dynamical symmetries of the model, because all the transitional bases are well localized

in the limiting ones. That is also why we do not need to analyze wave-function entropies of the rest of the Casten triangle in the whole (continuous!) set of all integrable bases — the results would be qualitatively the same as with the dynamical-symmetry bases alone. This argument holds true even in more general cases if the integrable region with no dynamical-symmetry is located on a transition between two chains (1) differing only by the subgroup  $G_i$ , as discussed in Sect. II B. Finally, it should be remarked that the simple fact of the common  $SO(5)$  subgroup along the  $U(5)$ – $SO(6)$  transition and its dynamical consequences remained overlooked for long [37], which is perhaps also a reason for the potential utility of entropy analyses.

The other non-chaotic (although not perfectly regular) region found in Refs. [16,17] is the strip connecting the  $U(5)$  and  $SU(3)$  vertices, but inside the triangle. It is also associated with an increased localization in the symmetry bases. One sees in Fig. 7 that a partial lowering of the  $r^{\mathcal{B}}$  values in this region (for  $\eta$  above, say, 0.5) is present in the  $U(5)$ ,  $SO(6)^*$ , and  $SO(6)$  histograms, and (for smaller  $\eta$ ) also in the  $SU(3)$  histogram. The effect is well visible in the product histogram. This behaviour clearly cannot be caused by some common subgroup, as in the previous case, and its explanation is still missing. Perhaps the newly introduced [27,38,39], so-called partial dynamical symmetries provide a possibility for such an explanation.

In Fig. 8 we compare the curve in the Casten triangle indicated in Ref. [17] as the bottom of the new semiregular valley with the corresponding chain of boxes with a minimum value of the entropy-ratio product  $R$ . The former, evaluated as the curve of a minimal fraction  $\sigma$  of the chaotic phase-space volume [17], is given essentially by the linear function  $\chi \approx [(\sqrt{7} - 1)\eta - \sqrt{7}]/2$  (see Fig. 13 in Ref. [17]). The overall agreement of the minimum- $R$  and minimum- $\sigma$  strips is good, indicating that standard chaotic measures and the entropy-ratio product express the same quality. Some deviations of the two strips are probably caused by the finite resolution of the grid in the  $R$ -plot, and by some uncertainty induced by the standard chaotic measures themselves (one could equally well use another measure than  $\sigma$ , yielding probably a slightly different curve). Also shown in Fig. 8 are the  $r^{\mathcal{B}}$  ratios and the

product  $R$  on the indicated section of the Casten triangle (note that this section does not correspond to a fixed value of  $\chi$ ; see the coordinate lines in Fig. 1). The passage of this section through chaotic and semiregular regions can be easily identified.

#### D. $L$ -dependence

In Ref. [15], the wave-function entropy was evaluated for angular momenta  $L=0, 10, 20$ , and 30. If the case of  $L=30$  is excluded, for which the dimension  $n$  is already substantially reduced due to the proximity of the upper angular-momentum limit  $L_{\max}=40$  for  $N=20$ , the entropy decreases with  $L$  (within the given set of  $L$ 's) in the whole range of the Casten triangle. This is in agreement with the work of Alhassid and Whelan [17], who observed an overall decrease of chaotic measures with angular momentum.

In Fig. 9, we present a detailed  $L$ -dependence of the average wave-function entropy ratios for all momenta between  $L=0$  and 20 for two particular points of the Casten triangle. The first one ( $\eta=1/10, \chi=-\sqrt{7}/4$ ) is located in the most chaotic region, while the other ( $\eta=1/2, \chi=0$ ) is on the regular U(5)–SO(6) edge. The previous result [15], based on the limited number of  $L$ 's, is confirmed now for all  $L \leq 20$ , but one should be aware that at some value of the angular momentum the entropy ratio has a minimum and turns growing (cf. Fig. 1 in Ref. [15]). Note that within the chosen interval of angular momenta the dimension  $n$  changes between limits  $n=33$  (for  $L=3$ ) and  $n=121$  ( $L=8, 10$ ).

One sees (in the upper two diagrams in Fig. 9) that the trend to decrease is common to all the five entropies. However, also apparent from Fig. 9 is the staggering of all entropy ratios, particularly strong for small angular momenta, which gives rise to large oscillations in the  $L$ -dependence of the entropy-ratio product  $R$  (lower two diagrams). This behaviour of the wave-function entropy, noticed already in Ref. [28] for a different IBM-1 parameterization, refers to an earlier observation made by Paar and Vorkapić [40] that within the IBM-1 the states with  $L=0, 3$  have larger spectral chaotic measures than those with  $L=2, 4$ . These findings are particularly interesting because similar dependence was identified [41] also in a

large experimental-data ensemble of nuclear levels.

### E. $N$ -dependence

Since the boson number  $N$  is, like  $L$ , a conserved quantum number, we shall study how the wave-function entropies vary with it. In general, because various  $\mathcal{C}_1[\text{U}(6)]=N$  eigenspaces carry various irreducible representations of the dynamical group, we ask how properties of the system depend on the particular choice of the model Hilbert space. An example of such a dependence was already mentioned in Sect. IV A (see Fig. 4).

An important question is whether the semiregular region inside the Casten triangle (see Sect. IV C) survives when changing  $N$ . The entropy-ratio product  $R$  of  $L=10$  states on the triangle section from Fig. 8 (the line parallel with the  $\text{SO}(6)$ – $\text{U}(5)$  side) is plotted in Fig. 10 for  $N=11, 14, 17$ , and  $20$ . All the  $R$ -plots have minima at about  $3/4$  of the  $\eta$ -range, indicating the passage of the given section through the semiregular region. It seems therefore that the semiregular strip is not just a large- $N$  effect, although for  $N=11$  the minimum is less pronounced relatively to the chaotic side regions in Fig. 10.

An interesting  $N$ -dependent effect appears in the  $\text{U}(5)$ – $\text{SO}(6)$  transitional region. We discussed already that the  $\text{U}(5)$ ,  $\text{SO}(6)$ , and  $\text{SO}(6)^*$  entropies are all suppressed in this region since a complete mixing of states is disabled by the common  $\text{SO}(5)$  symmetry. Consequently, any purely  $\text{U}(5)$ – $\text{SO}(6)$  transitional hamiltonian has a block-diagonal structure in the  $\text{U}(5)$ ,  $\text{SO}(6)$ , and  $\text{SO}(6)^*$  bases [36], each block corresponding to fixed  $\text{SO}(5)$  quantum numbers  $v$  and  $n_\Delta$  [12]. In Fig. 11, we show the  $N$ -dependence of the average dimension  $n_{\text{block}}$  of these blocks for  $L=10$  (individual block dimensions coincide with the degeneracy dimensions  $n_{\text{deg}}^{(i)}$  from Eq. (8)) relative to the total dimension  $n$  of the  $L=10$  subspace. The relative block dimension  $n_{\text{block}}/n$  naturally decreases with  $N$  as the number of blocks (number of allowed  $(v, n_\Delta)$ -values) increases, which yields an  $\approx 1/N$  dependence for large  $N$  and  $L \ll N$ .

It is clear that the decrease of the relative average block dimensions on the  $\text{U}(5)$ – $\text{SO}(6)$  edge with  $N$  reduces increasingly also the corresponding GOE-normalized entropies in the

U(5), SO(6), and SO(6)\* bases. Consequently, in the  $N \rightarrow \infty$  limit the whole integrable U(5)–SO(6) region would yield the above three normalized entropies equal to zero. This is also illustrated in Fig. 11. The quantity that can be directly compared with the average block dimension is the average effective number of wave-function components  $n_{\text{eff}}^{\mathcal{B}} = \exp W^{\mathcal{B}}$  (see Sect. III D). Open squares and triangles in Fig. 11 indicate values of  $n_{\text{eff}}^{\text{SO}(6)*}/n$  for  $L=10$  eigenstates at the U(5) and SO(6) vertices. Note that  $n_{\text{eff}}^{\text{SO}(6)}$  at the U(5) vertex and  $n_{\text{eff}}^{\text{U}(5)}$  at the SO(6) vertex are determined by the given SO(6)\* values since the relation  $W^{\text{SO}(6)*}(L, N, \eta=1, \chi=0) = W^{\text{SO}(6)}(L, N, \eta=1, \chi=0) = W^{\text{U}(5)}(L, N, \eta=0, \chi=0)$  is valid for average entropies from Eq. (9). Here, the first equality follows from the fact that the expansion of the SO(6) and SO(6)\* eigenstates in the U(5) basis differ only by phases (each U(5) eigenstate has a sharp number of s- and d-bosons) and the second equality from the evident rule that  $\mathcal{B}$ -expansion matrix of  $\mathcal{B}'$  is just a Hermitian conjugate of the  $\mathcal{B}'$ -expansion matrix of  $\mathcal{B}$ . As can be seen from Fig. 11, the average U(5), SO(6) and SO(6)\* relative numbers of wave-function components at the U(5)–SO(6) edge directly follow the decrease of the relative block dimensions.

## V. CONCLUDING REMARKS

In this work we attempted to find a continuous measure of the dynamical-symmetry content for a class of IBM-1 hamiltonians, and relate it to the variety of transitional degrees between regularity and chaos that the hamiltonians exhibit. The key ingredient of our analysis was the simple observation that any dynamical symmetry is connected with a certain subset of bases, for which the average overlap with eigenbases of the tested hamiltonians can be measured by the wave-function entropy. This provided us a tool for studying various phenomena accompanying the process of dynamical-symmetry breaking (Sect. IV).

We faced the following basic problems: *(i)* Removal of the dimension-dependence of the average wave-function entropy by normalization. It is essential if the entropy values for subsets of eigenstates with different conserved quantum numbers ( $N$  and  $L$  in our case) are



to be compared. It turned out that the GOE normalization (Sect. 9) is quite satisfactory. *(ii)* Uncertainty of the reference dynamical-symmetry bases for non-canonical group reductions. This problem was shown to be of minor importance for the IBM-1 (Sect. III B), but can be more serious for other models, for which the uncertainty should therefore be rigorously taken into account. *(iii)* Construction of the entropy-ratio product in Eq. (12). It remains to be an *ansatz*, but seems to work reasonably well. *(iv)* Necessity to consider also the “hidden” dynamical symmetries, such as  $SU(3)^*$  and  $SO(6)^*$  [15]. Note that these symmetries arise, in general [14], from inner automorphisms of the dynamical group and are not classified by the group theory. *(v)* The fact that not all integrable hamiltonians of the system are connected with dynamical symmetries. It means that not all potentially relevant reference bases can be constructed by group methods. Nevertheless, in the above-discussed case of the  $U(5)$ – $SO(6)$  transition (Sects. II B, IV C) the regular dynamics was identified by means of only the dynamical-symmetry bases.

The most important goal of this work was to establish a link between the dynamical-symmetry content and the degree of regularity/chaos. It turned out (Sect. IV E, F) that for the simple model under study the wave-function entropies are indeed strongly correlated with the standard chaotic measures used, for instance, in Ref. [17]. If the same conclusion can be repeated also for other dynamical systems, the present approach would provide a new measure of chaos, additional to the standard ones. It is clear that the dynamical-symmetry content expressed by the overlap of bases measures, in fact, to what extent the integrals of motion attached to the reference dynamical symmetry remain approximate integrals of motion for the tested system. In this connection, it would be interesting to know whether also sets of some approximate or exact (?) integrals of motion, not arising from any of the dynamical symmetries of the system, exist and are important<sup>1</sup>. These questions should be

---

<sup>1</sup> For example, the integrable  $U(5)$ – $SO(6)$  systems do not possess any dynamical symmetry but their integrals of motion — including the hamiltonian — can be constructed solely from the integrals

addressed in next studies.

Finally, it should be stressed that we do not pretend to find an analytical definition of any sort of generalized symmetry, such as the partial dynamical symmetry [38], for instance. Our numerical analysis allows one to see, whether the content of a particular dynamical symmetry is small or large, but cannot answer why it is so. Nevertheless, even with the above limitations in mind we believe that the approach presented in this work can yield a new probe for investigating dynamical properties of finite quantum systems.

### ACKNOWLEDGEMENTS

The work was supported by the internal grant No. 38/97 of the Charles University and by the Swiss National Science Foundation. P.C. acknowledges an additional support from the University of Fribourg.

---

corresponding to dynamical symmetries — see Eq. (5).

## REFERENCES

- [1] M.C. Gutzwiller, *Chaos in Classical and Quantum Mechanics* (Springer-Verlag, New York, 1990).
- [2] T.A. Brody *et al.*, *Rev. Mod. Phys.* **53**, 385 (1981); T. Guhr, A. Müller–Groeling, and H.A. Weidenmüller, to appear in *Phys. Rep.*
- [3] M.L. Mehta, *Random Matrices* (Academic Press, San Diego, London, 1990).
- [4] H. Feshbach, *Physics Today*, April 1986, p. 7.
- [5] O. Castaños, A. Frank, and R. Lopez-Peña, *J. Phys. A* **23**, 5141 (1990).
- [6] A. Frank and P. Van Isacker, *Algebraic Methods in Molecular and Nuclear Structure Physics* (John Willey & Sons, New York, 1994).
- [7] D.J. Rowe, *Prog. Part. Nucl. Phys.* **37**, 265 (1996).
- [8] W.M. Zhang, C.C. Martens, D.H. Feng, and J.M. Yuan, *Phys. Rev. Lett.* **61**, 2167 (1987).
- [9] W.M. Zhang, D.H. Feng, J.M. Yuan, and S.J. Wang, *Phys. Rev. A* **40**, 438 (1989).
- [10] W.M. Zhang, D.H. Feng, and J.M. Yuan, *Phys. Rev. A* **42**, 7125 (1990).
- [11] W.M. Zhang and D.H. Feng, *Phys. Rep.* **252**, 1 (1995).
- [12] F. Iachello and A. Arima, *The Interacting Boson Model* (Cambridge University Press, Cambridge, 1987).
- [13] P. Van Isacker, A. Frank, and J. Dukelsky, *Phys. Rev. C* **31**, 671 (1985).
- [14] D. Kusnezov, *Phys. Rev. Lett.* **79**, 537 (1997).
- [15] P. Cejnar and J. Jolie, *Phys. Lett. B* **420**, 241 (1998).
- [16] Y. Alhassid and N. Whelan, *Phys. Rev. Lett.* **67**, 816 (1991).

- [17] N. Whelan and Y. Alhassid, Nucl. Phys. **A556**, 42 (1993).
- [18] Y. Alhassid, A. Novoselsky, and N. Whelan, Phys. Rev. Lett. **65**, 2971 (1990).
- [19] Y. Alhassid and N. Whelan, Phys. Rev. C **43**, 2637 (1991).
- [20] Y. Alhassid and A. Novoselsky, Phys. Rev. C **45**, 1677 (1992).
- [21] R.L. Hatch and S. Levit, Phys. Rev. C **25**, 614 (1982).
- [22] E. López-Moreno and O. Castaños, Phys. Rev. C **54**, 2374 (1996).
- [23] R. Blümel and U. Smilansky, Phys. Rev. Lett. **52**, 137 (1984).
- [24] F. Iachello and R. Levine, Europhys. Lett. **4**, 389 (1987).
- [25] F.M. Izrailev, Phys. Lett. A **134**, 13 (1988).
- [26] J. Reichl, Europhys. Lett. **6**, 669 (1988).
- [27] N. Whelan, Y. Alhassid and A. Leviatan, Phys. Rev. Lett. **71**, 2208 (1993).
- [28] J. Jolie, in Perspectives for the Interacting Boson Model, ed. R.F. Casten *et al.* (World Scientific, Singapore, 1994) p.45.
- [29] V. Zelevinsky, M. Horoi and B.A. Brown, Phys. Lett. B **350**, 141 (1995).
- [30] M. Horoi, V. Zelevinsky and B.A. Brown, Phys. Rev. Lett. **74**, 5194 (1995).
- [31] V. Zelevinsky, Annu. Rev. Nucl. Part. Sci. **46**, 237 (1996).
- [32] V. Zelevinsky, B.A. Brown, N. Frazier, M. Horoi, Phys. Rep. **276**, 85 (1996).
- [33] V. Paar, D. Vorkapić, and A.E.L. Dieperink, Phys. Rev. Lett. **69**, 2184 (1992).
- [34] B. Lauritzen, Y. Alhassid, and N. Whelan, Phys. Rev. Lett. **72**, 2809 (1994).
- [35] R.F. Casten, N.V. Zamfir, and D.S. Brenner, Phys. Rev. Lett. **71**, 227 (1993).
- [36] T. Mizusaki, N. Yoshinaga, T. Shigehara, and T. Cheon, Phys. Lett. B **269**, 6 (1991).

- [37] A. Leviatan, A. Novoselsky, and I. Talmi, Phys. Lett. B **172**, 144 (1986).
- [38] Y. Alhassid and A. Leviatan, J. Phys. A: Math. Gen. **25**, L1265 (1992).
- [39] A. Leviatan and N.D. Whelan, Phys. Rev. Lett. **77**, 5202 (1996).
- [40] V. Paar and D. Vorkapić, Phys. Lett. B **205**, 7 (1988).
- [41] A.Y. Abul-Magd and H.A. Weidenmüller, Phys. Lett. B **162**, 223 (1985).

TABLES

TABLE I. Definitions of the IBM-1 operators in the convention used in this work.

$\hat{N} = s^\dagger s + d^\dagger \cdot \tilde{d}$	$\hat{n}_d = d^\dagger \cdot \tilde{d}$
$\hat{L} = \sqrt{10}[d^\dagger \times \tilde{d}]^{(1)}$	$\hat{Q}_\chi = [d^\dagger \times s + s^\dagger \times \tilde{d}]^{(2)} + \chi[d^\dagger \times \tilde{d}]^{(2)}$
$\hat{P}_\phi^\dagger = s^\dagger s^\dagger - e^{i\phi} d^\dagger \cdot d^\dagger$	
$\hat{C}_1[\text{U}(5)] = \hat{n}_d$	$\hat{C}_2[\text{U}(5)] = \hat{n}_d(\hat{n}_d + 4)$
$\hat{C}_2[\text{SO}(6)] = \hat{N}(\hat{N} + 4) - \hat{P}_\pi^\dagger \hat{P}_\pi$	$\hat{C}_2[\text{SU}(3)] = 2\hat{Q}_{-\frac{\sqrt{3}}{2}} \cdot \hat{Q}_{-\frac{\sqrt{3}}{2}} + \frac{3}{4}\hat{L} \cdot \hat{L}$
$\hat{C}_2[\text{SO}(5)] = \hat{n}_d(\hat{n}_d + 3) - (d^\dagger \cdot d^\dagger)(\tilde{d} \cdot \tilde{d})$	$\hat{C}_2[\text{SO}(3)] = \hat{L} \cdot \hat{L}$

TABLE II. Degeneracy factors  $f_{\text{deg}}$  from Eq. (8) characterizing the uncertainty of the IBM-1 eigenbases in the dynamical-symmetry limits for various boson numbers  $N$  and angular momenta  $L$ . Note that for  $L=0$  all the  $f_{\text{deg}}$  values are equal to 0. There is just one  $L=30$  state for  $N=15$ .

		$L = 10$	$L = 20$	$L = 30$
$N = 15$	U(5),SO(6),SO(6)*	1.3 %	3.3 %	—
	SU(3),SU(3)*	4.3 %	7.5 %	—
$N = 20$	U(5),SO(6),SO(6)*	0.7 %	2.0 %	3.3 %
	SU(3),SU(3)*	2.5 %	3.6 %	7.5 %
$N = 25$	U(5),SO(6),SO(6)*	0.4 %	1.1 %	2.0 %
	SU(3),SU(3)*	1.7 %	2.3 %	3.6 %

## FIGURES

FIG. 1. Mapping of the  $(\eta, \chi)$ -parameter space of Eq. (4) onto a triangle (left) and its relation to an ideal Casten triangle (right). Hamiltonians with non-standard dynamical symmetries (3) are absent from the present parameterization.

FIG. 2. Classical potential (6) as a function of quadrupole variables  $\beta$  and  $\gamma$  for six  $(\eta, \chi)$  parameter pairs (A...F) from various parts of the Casten triangle.

FIG. 3. Quantities characterizing the GOE distribution of the average wave-function entropy for dimensions  $n \leq 30$  (see text).

FIG. 4. The U(5)-symmetry breaking in the region  $0.5 \leq \eta \leq 1$  for two boson numbers (top *vs* bottom). Left: the average U(5)-entropy ratio from Eq. (11) for all  $L=0$  states. Middle: the ground-state's U(5)-entropy ratio. Right: the admixture of the U(5) ground state in the real ground state. Points outside the Casten triangle are filled with zeros.

FIG. 5. The U(5) (top) and SU(3) (bottom) wave-function entropy of individual  $L=10$  states along the U(5)–SU(3) transition ( $\eta=1 \rightarrow 0$ ,  $\chi=-(7/4)^{1/2}$ ). The state index  $\alpha$  is assigned increasingly with the state energy.

FIG. 6. A smoothed density of  $L=10$  states ( $N=20$ ) along the U(5)–SU(3) transition as a function of energy  $E$  (top) and the state index  $\alpha$  (bottom).

FIG. 7. The average-entropy ratios from Eq. (11) and their product from Eq. (12) for  $L=10$  states ( $N=20$ ) calculated over the whole range of the Casten triangle. The first five histograms display  $r^{\mathcal{B}}$  for the five dynamical-symmetry bases, while the lower right histogram represents the renormalized product  $R$ . Like in Fig. 4, points outside the triangle are filled with zeros.

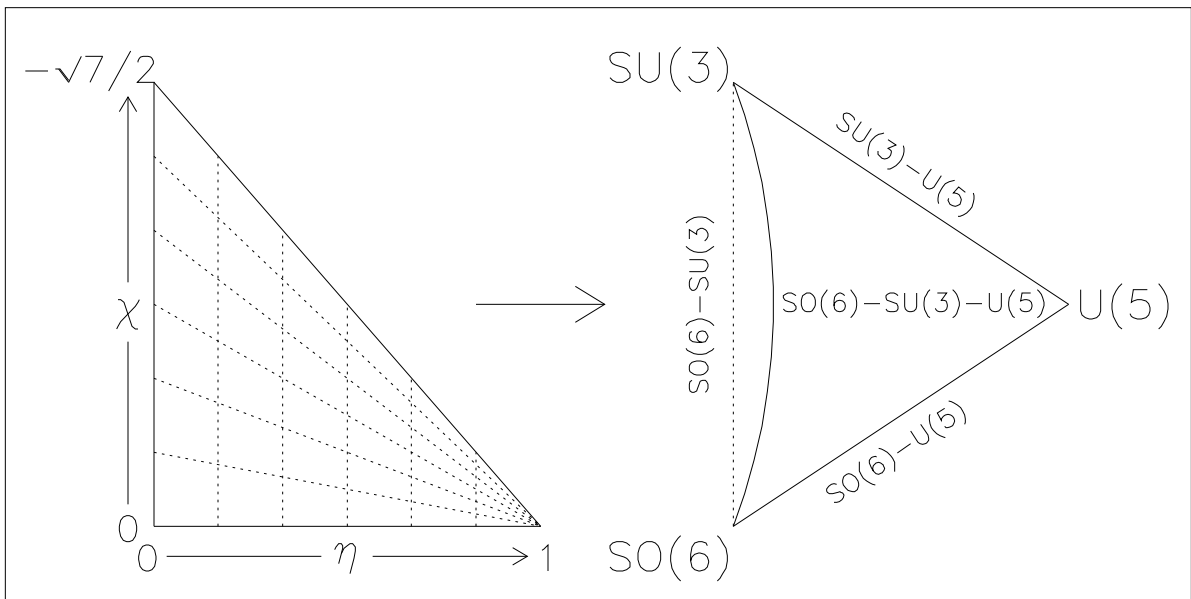
FIG. 8. The semiregular region inside the Casten triangle as deduced from classical chaotic measures (the fraction  $\sigma$  of the chaotic phase-space volume) and from the wave-function entropies (for  $L=10$  states with  $N=20$ ). Top: The bent curve indicates the  $(\eta, \chi)$ -localization of the  $\sigma$ -valley determined in Ref. [17], while boxes represent local minima (if any) of the entropy-ratio product  $R$  from Eq. (12). Bottom: Values of  $r^{\mathcal{B}}$ , see Eq. (11), and  $R$  along the given section (the dashed line above) of the Casten triangle.

FIG. 9. The angular-momentum dependence ( $L=0 \dots 20$ ) of the wave-function entropy for two points of the Casten triangle (left *vs* right). The five  $\mathcal{B}=\text{U}(5) \dots \text{SO}(6)^*$  average-entropy ratios  $r^{\mathcal{B}}$  are shown in the upper graphs and their product  $R$  in the corresponding lower graphs.

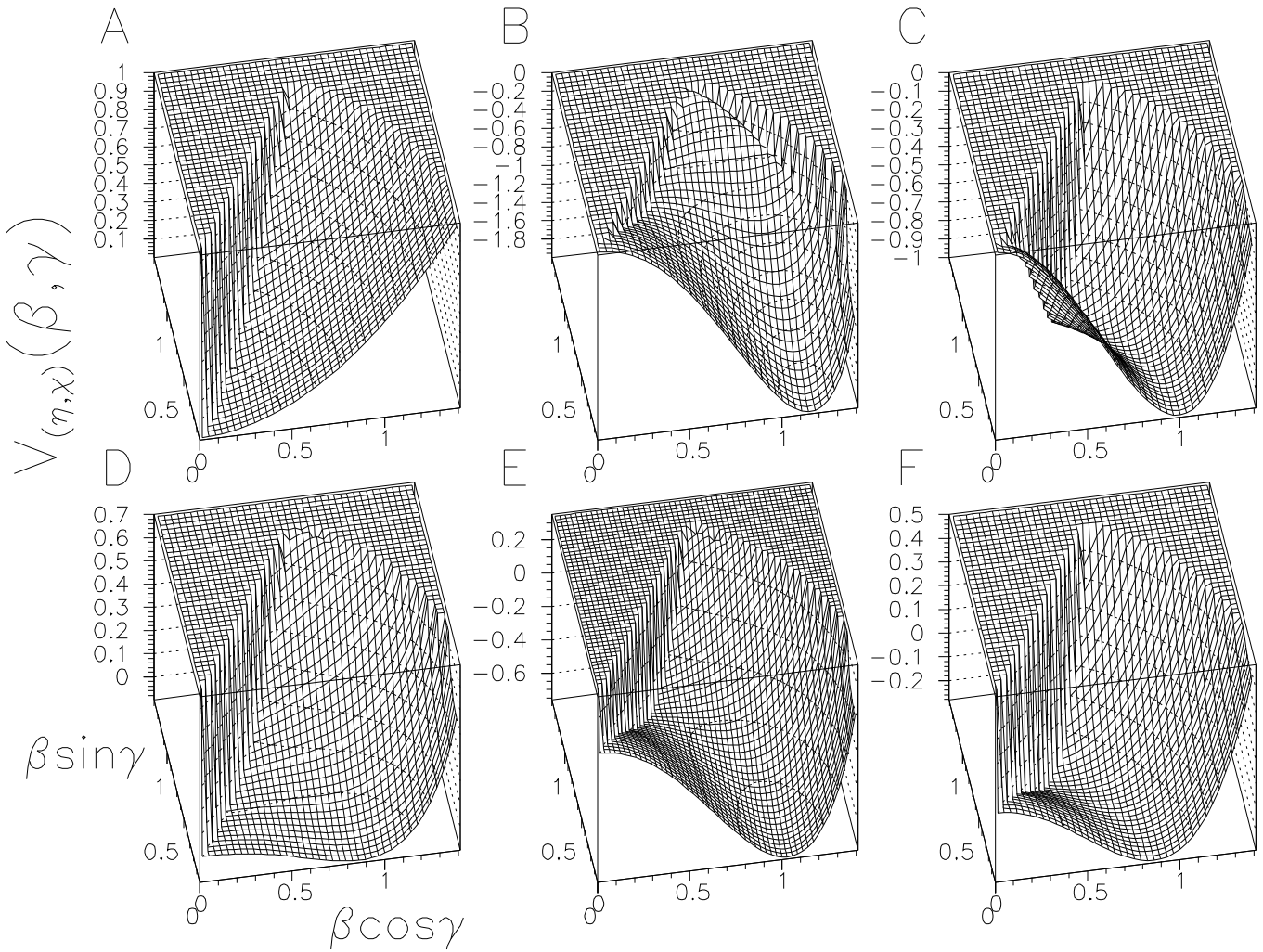
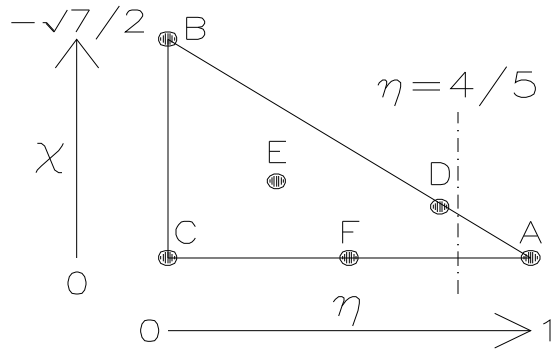
FIG. 10. The entropy-ratio product  $R$  along the  $\chi=0.54/(1-\eta)$  section of the Casten triangle (see the dashed line in Fig. 8–top) for  $L=10$  and various boson numbers  $N$  (cf. Fig. 8–bottom). The normalization of all  $R$ -plots is the same except for the  $N=11$  one, which should be multiplied by 2.

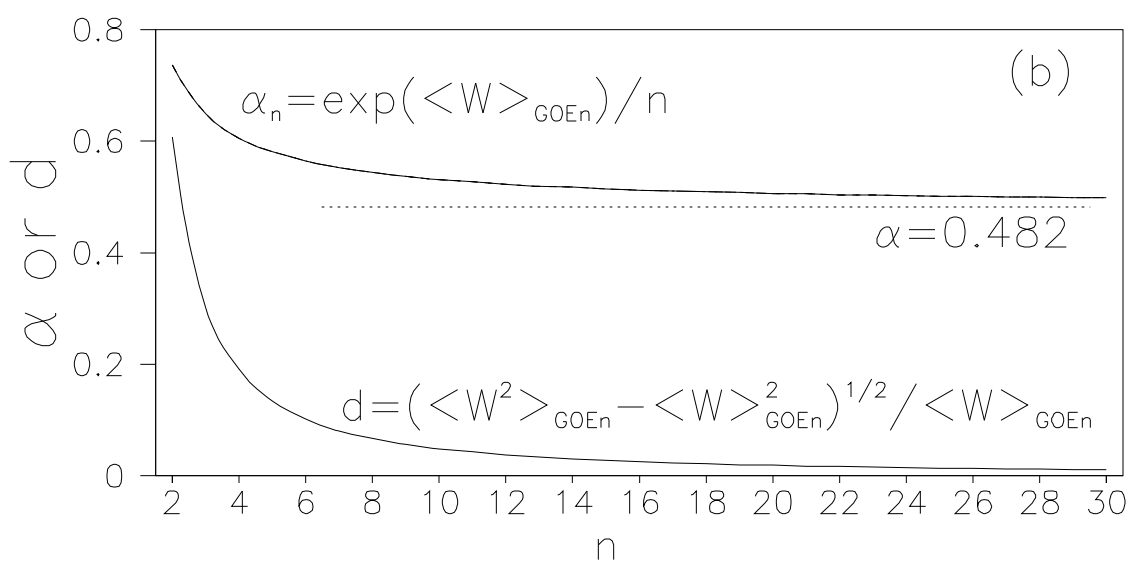
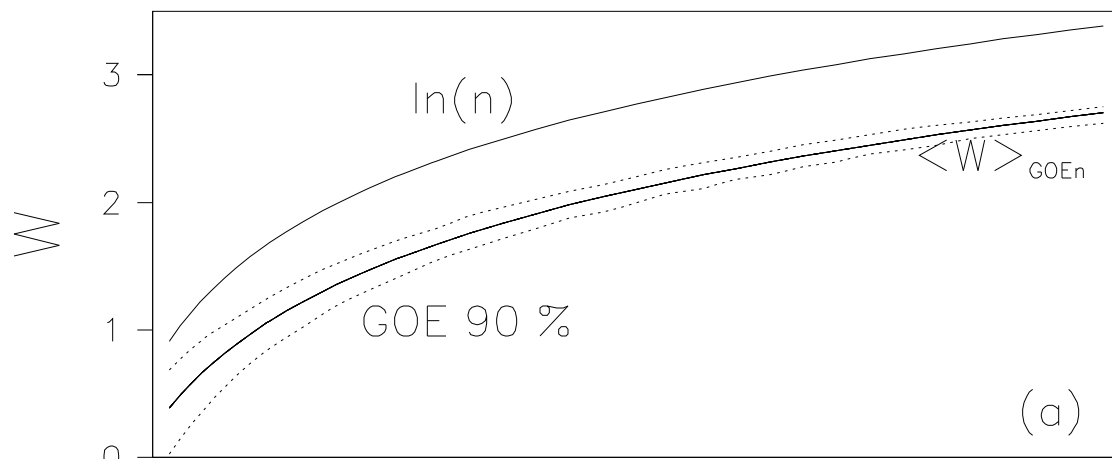
FIG. 11. The boson-number dependence of the relative average block dimension  $n_{\text{block}}/n$  of the block-diagonal (in the  $\text{U}(5)$ ,  $\text{SO}(6)$  and  $\text{SO}(6)^*$  bases) hamiltonians at the  $\text{U}(5)$ – $\text{SO}(6)$  transition for  $L=10$ . The average relative numbers of wave-function components  $n_{\text{eff}}^{\text{SO}(6)^*}/n$  are given separately for pure  $\text{U}(5)$  and  $\text{SO}(6)$  hamiltonians at five values of  $N$ . Total numbers  $n$  of the  $L=10$  states for each  $N$  are indicated inside the frame.





- A...  $\eta=1, \chi=0$
- B...  $\eta=0, \chi=-\sqrt{7}/2$
- C...  $\eta=0, \chi=0$
- D...  $\eta=3/4, \chi=-\sqrt{7}/2$
- E...  $\eta=1/3, \chi=-\sqrt{7}/4$
- F...  $\eta=1/2, \chi=0$





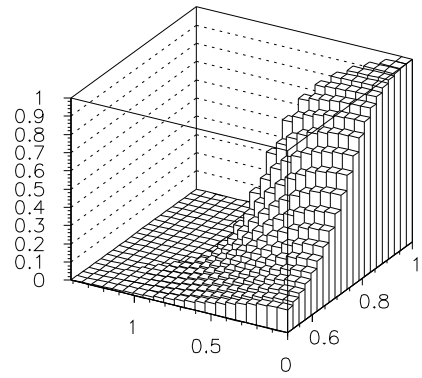
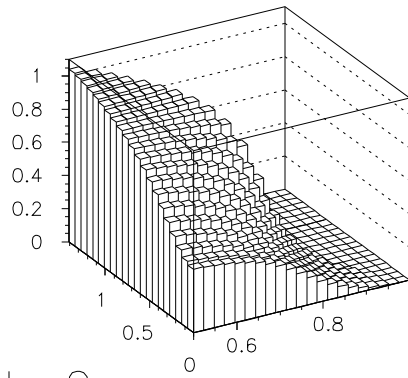
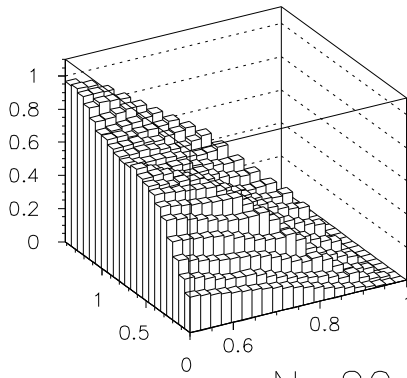
$$r^{U(5)}$$

$$r_1^{U(5)}$$

$$|a_{11}^{U(5)}|^2$$

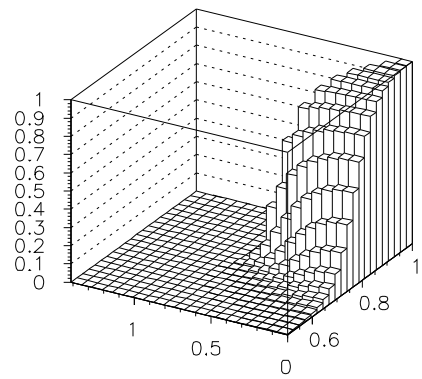
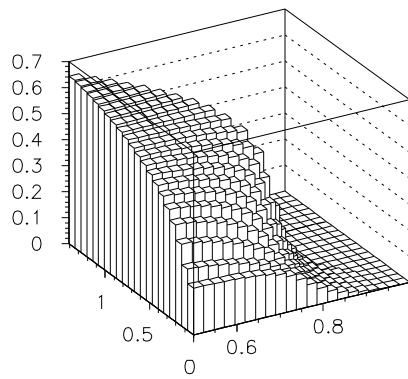
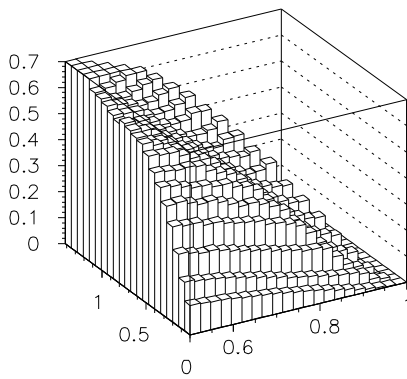
n=19

N=10, L=0



n=44

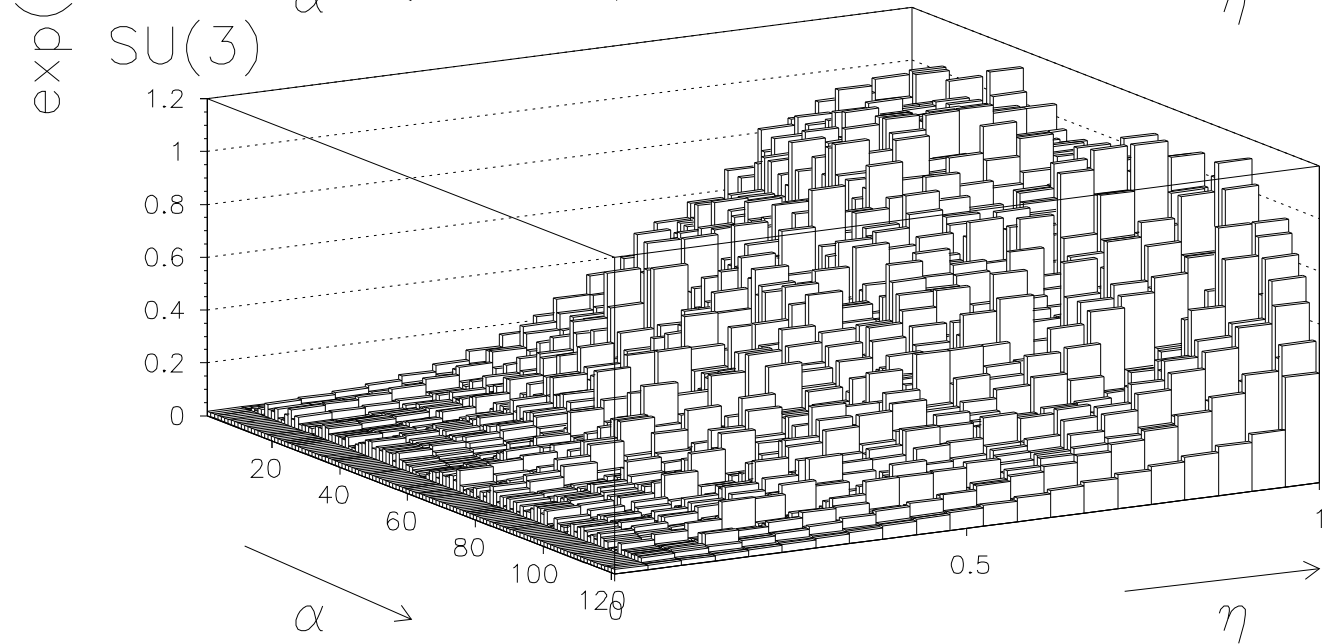
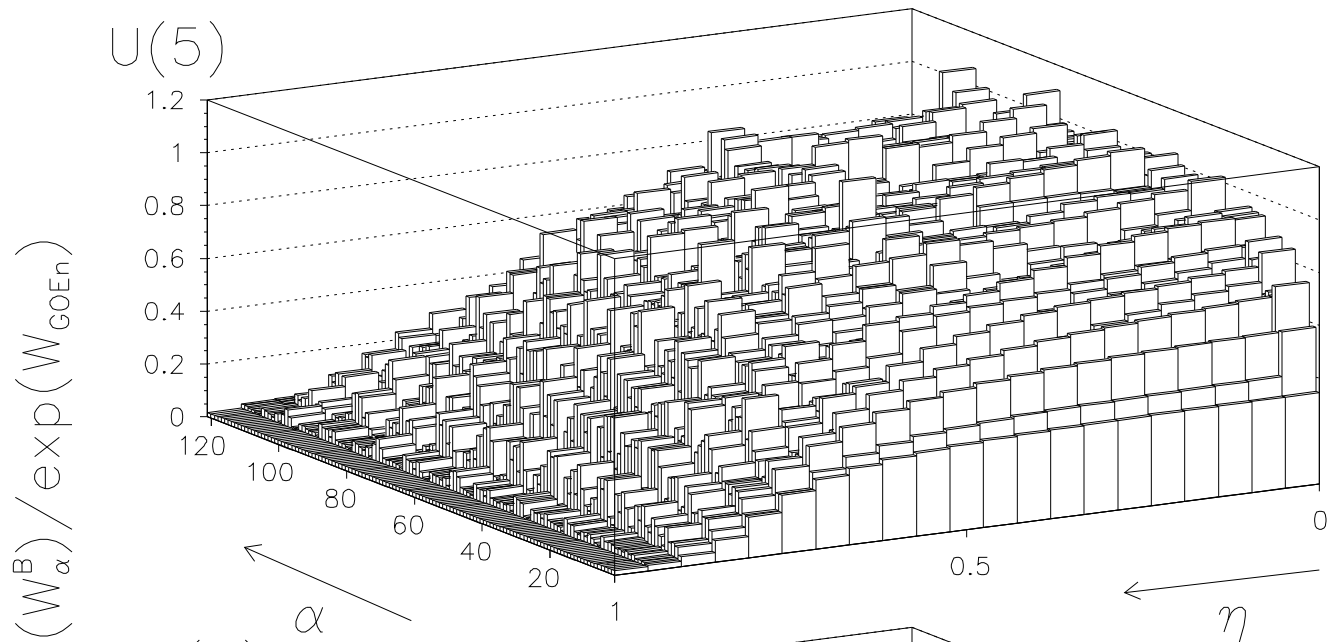
N=20, L=0



$N=20$

$L=10$

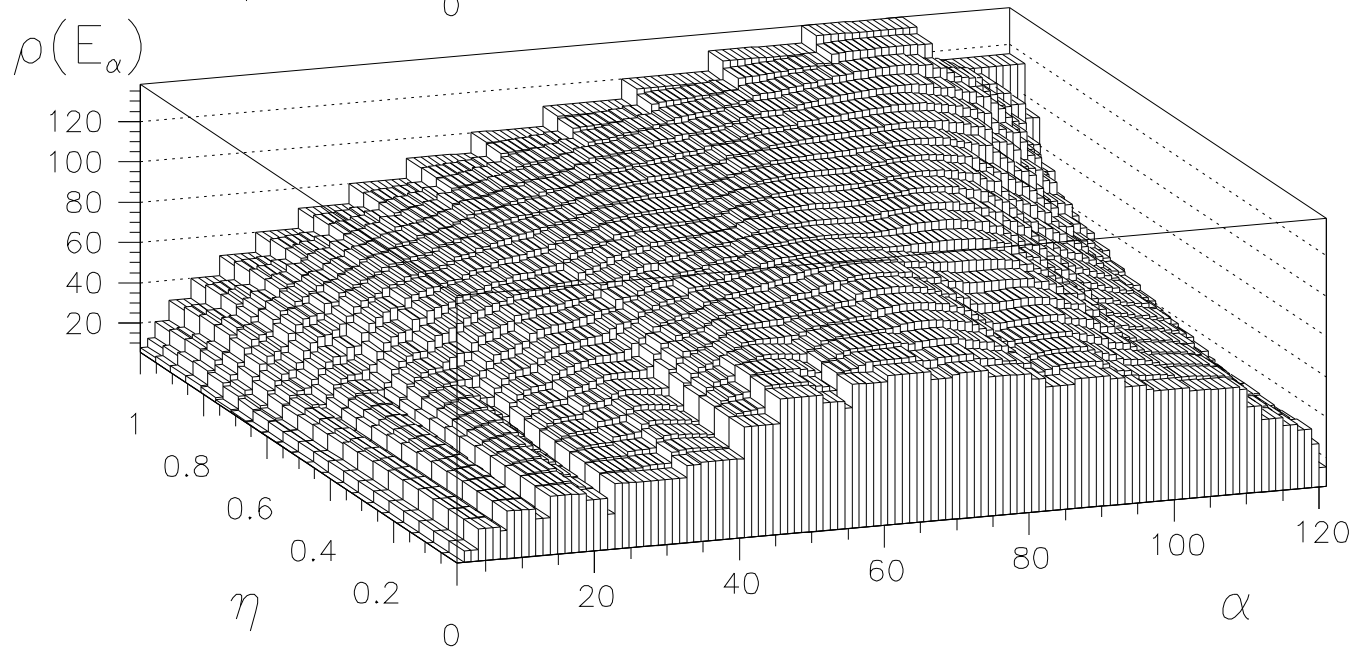
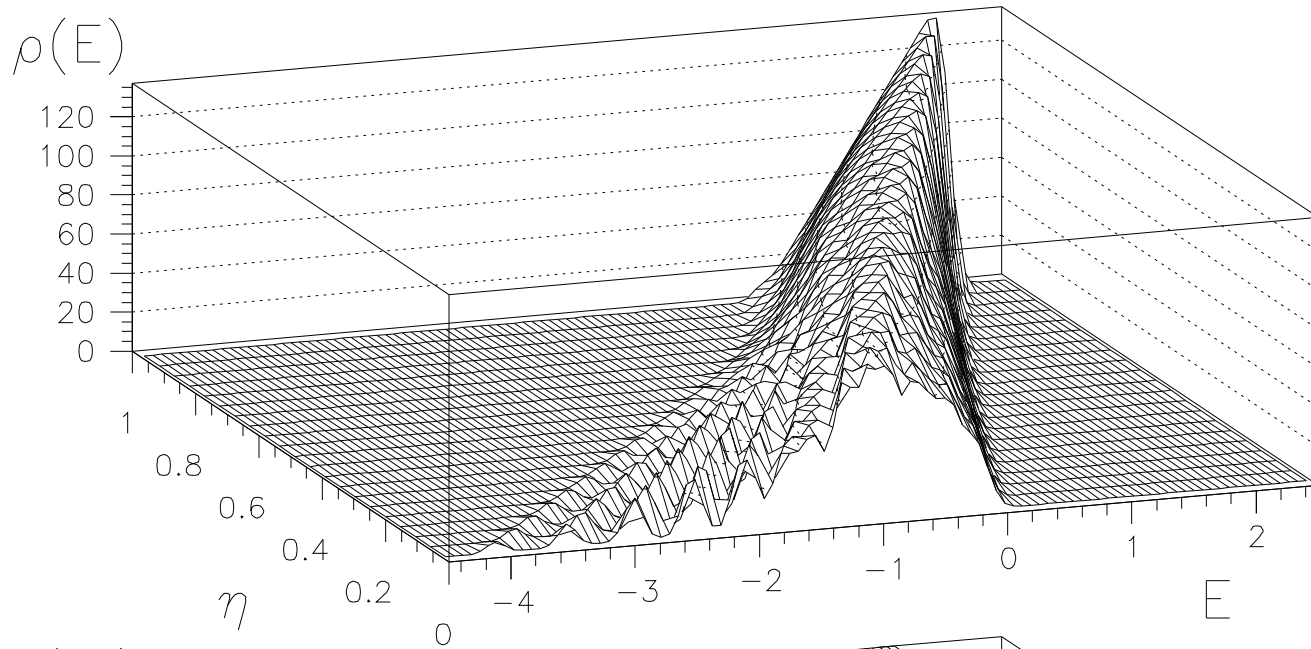
$n=121$



$N=20$

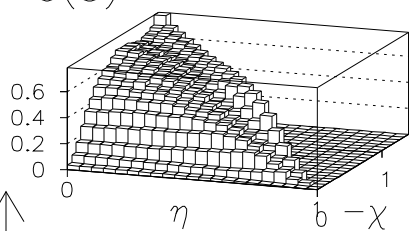
$L=10$

$n=121$

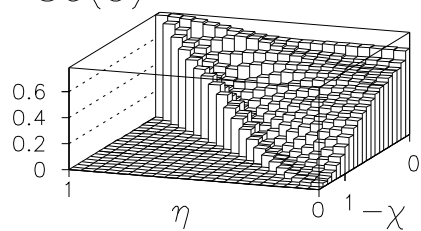


$N=20, L=10$  ( $n=121$ )

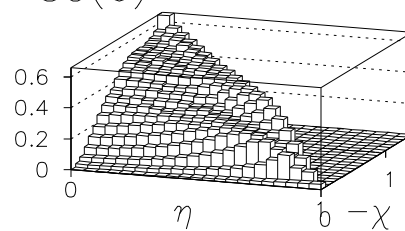
U(5)



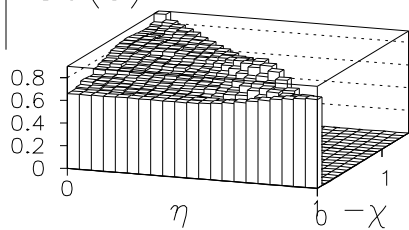
SU(3)



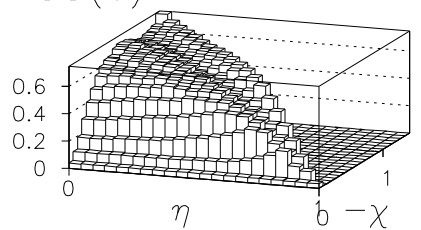
SO(6)



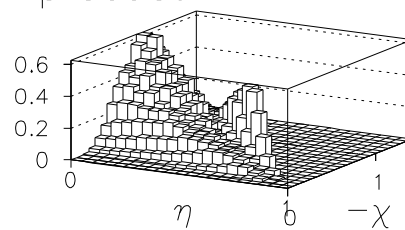
$\uparrow$   
B  
SU(3)\*

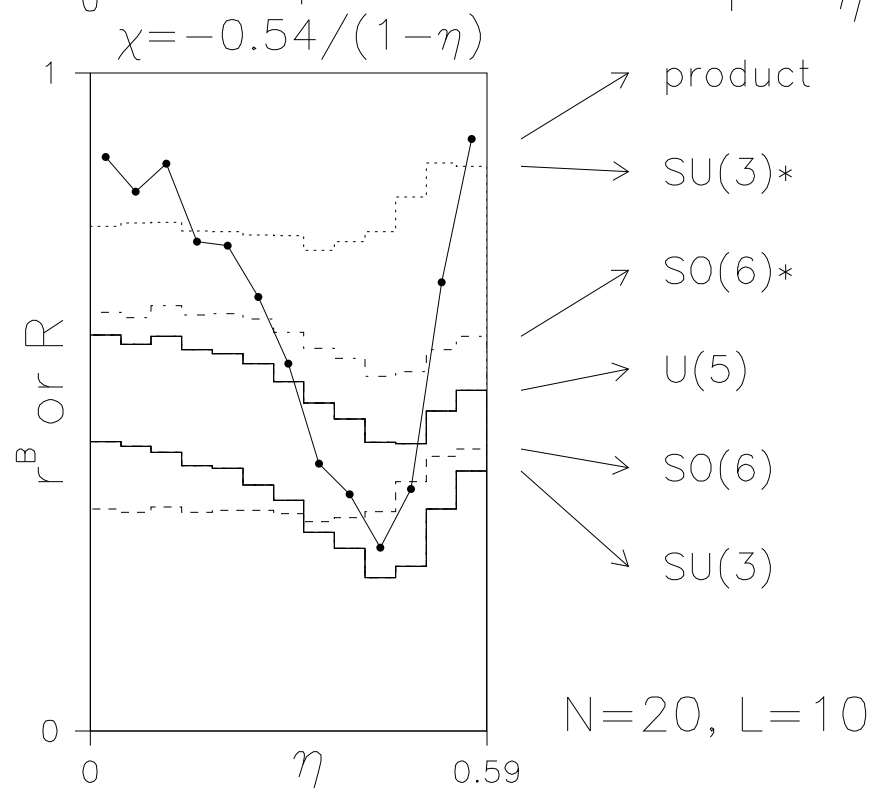
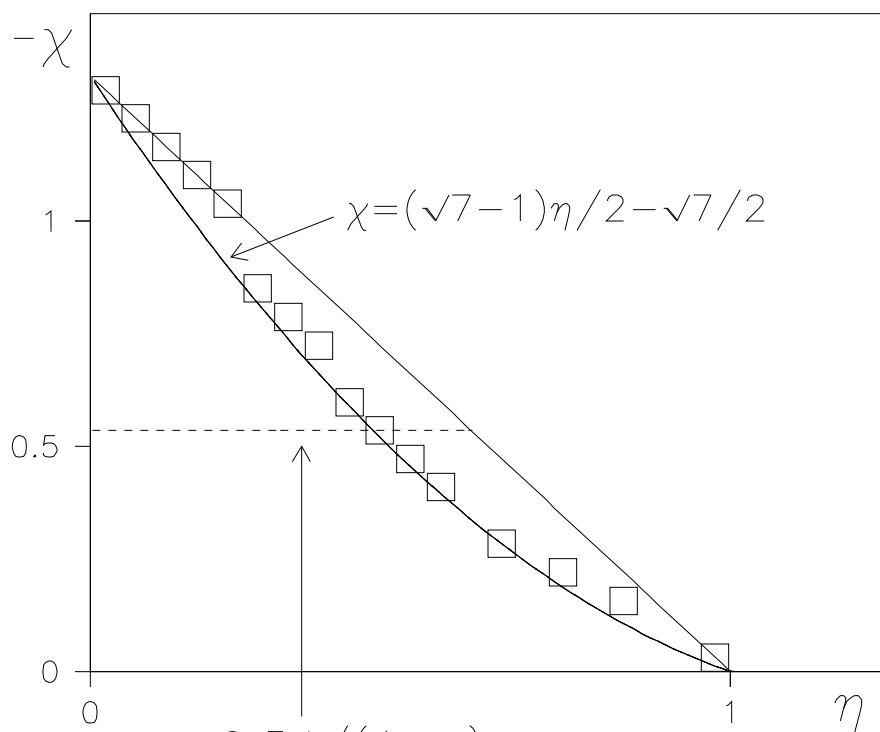


SO(6)\*



product

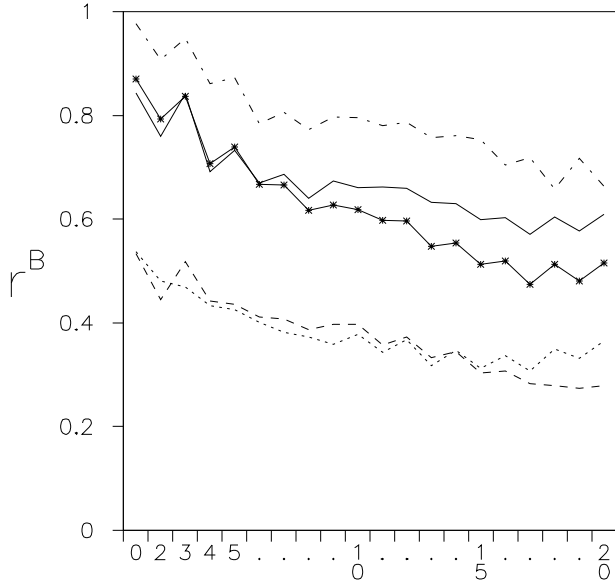




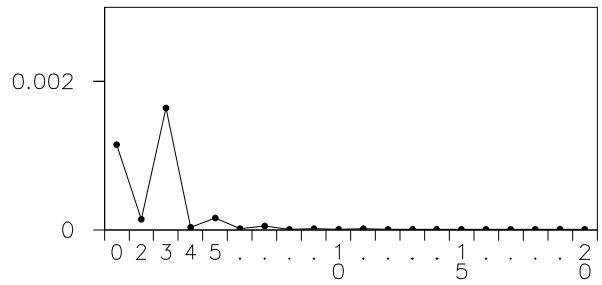
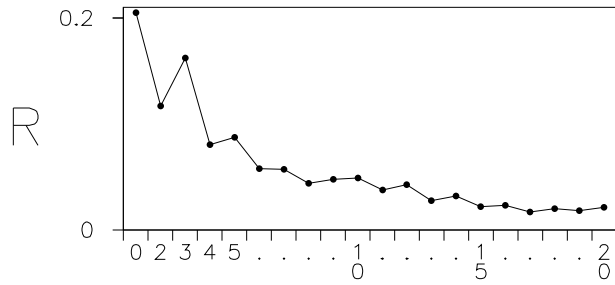
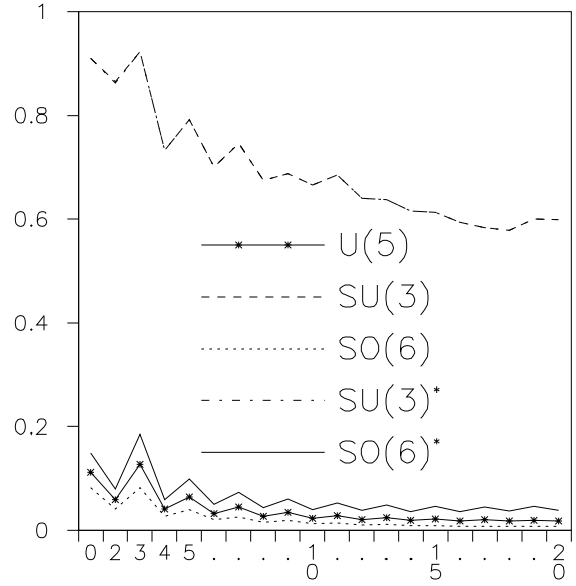


N=20

$\eta=1/10, \chi=-\sqrt{7}/4$



$\eta=1/2, \chi=0$



L

